J. Fluid Mech. (1981), *vol.* 113, *pp.* 333–346
Printed in Great Britain

Methane oxidation near a cold wall

By R. KEIPER AND J. H. SPURK

Fachgebiet Technische Strömungslehre, 6100 Darmstadt,
Petersenstrasse 30, W. Germany

(Received 4 July 1980 and in revised form 21 April 1981)

The thermal non-equilibrium boundary layer at the end wall of a shock tube in methane combustion initiated by a reflected shock, is investigated theoretically and experimentally. Time-dependent boundary conditions are caused by the shock–boundary-layer interaction and the combustion process outside the boundary layer, and are taken into account. Space- and time-resolved density measurements using a focused laser beam are in good agreement with results from numerical computation and show existence of similarity solutions for short and long times. Differences, so far unexplained, occur between measured and predicted heat fluxes to the wall.

1. Introduction

In this paper we report on the computation of a laminar, thermal boundary layer, which develops near a plane wall when a shock reflected from this wall ignites a combustible mixture of gases. Near the wall the chemical relaxations are substantially influenced by diffusion and heat conduction when time is comparable to the chemical relaxation times.

Such a flow can be realized experimentally in a shock tube, when the shock is reflected from the end wall of the tube. This boundary-layer flow has a certain practical appeal since it may serve as a model for the boundary-layer flow in an internal-combustion piston engine. Of course, there are obvious and important differences: the boundary layer may well be turbulent in the case of the piston engine and the outside flow is quite different. Despite these differences, one of the essential features of the boundary layer, namely the coupling of the chemical reactions with transport processes, are common to both of these flows.

The thermal boundary layer at the shock tube end wall has been computed by Fay & Kemp (1965) for an ionized monatomic gas in the limiting cases that the gas in the boundary layer is either frozen or at equilibrium. These flows are self-similar for time-independent boundary conditions at the wall and far away from the wall. However, the idealized conditions of time-independent and homogeneous flow behind the reflected shock, are not met in shock tube experiment, even if the outer flow is non-reacting. In a shock-initiated combustion there are a number of processes and this causes deviations from the ideal conditions. The energy producing reactions (i.e. the combustion proper) actually set in a certain time after the shock has passed a fixed station.

During this ignition delay time, shock reflection and the flow behind the shock are determined initially by the boundary-layer development at the end wall through the negative displacement effects of heat transfer to the wall (Sturtevant & Slachmuylders

1964). This effect dies out quite rapidly (Baganoff 1965), ($\sim 1\ \mu$s for the condition of our experiment) and is of no interest in the context of this paper. This applies *a fortiori* to molecular effects, such as temperature jump. Then at later times, vibrational relaxation behind the reflected shock (in our experiment vibration of the oxygen component) causes an increase in density. This disturbance overlaps with the disturbances due to the boundary layer behind the incident shock. There are two opposing effects. The first is the direct interaction of the reflected shock with the boundary layer, discussed first by Mark (1953). This interaction process causes a pressure drop behind the reflected shock. After the reflected shock has travelled some distance, conditions near the wall are mainly affected by small disturbances created by the boundary-layer growth behind the incident shock. These are amplified by the reflected shock, and as a result the pressure rises (Rudinger 1961; Dyner 1966).

After ignition delay, the combustion process generates pressure waves, which now strongly influence the flow field behind the shock. A realistic boundary layer computation must consider these effects and take the time dependent boundary conditions into account.

Fortunately, the changes of boundary conditions due to the side-wall boundary layer are so slow, as our experiments show, that the boundary-layer development is quasi-similar in a sense discussed later. The changes of the boundary conditions due to the combustion process occur with a typical time comparable to the diffusion time; the time-dependent conditions must be prescribed.

These were determined on the basis of one-dimensional unsteady reacting flow by the method of characteristics (Presley & Hanson 1969) or alternatively by assuming homogeneous flow and using one variable of state (density) from measurements.

The possible application to internal combustion engine requires the computation for a multi-component gas mixture. We compute the combustion of methane in air (in an argon heat bath) using the reaction mechanism of Bowman (1974) and the Zel'dovich mechanism as given by Nelson (1976). The transport coefficients for the boundary-layer solution are determined from kinetic theory on the basis of Lennard-Jones potentials.

We shall compare time- and space-resolved measurements of the refractive index in the thermal boundary layer and heat transfer to the end wall with the corresponding results from the numerical computation.

2. Boundary-layer equations

The equations which describe the boundary-layer flow normal to an infinite wall located at $x = 0$ may be taken from Fay & Kemp (1965). We give these equations in the co-ordinates

$$\eta = \left(\frac{c_{p0}}{2\lambda_0\rho_0 t}\right)^{\frac{1}{2}} \int_0^x \rho\, dx, \tau = t/\tau_r; \quad \tau_r = \left(\frac{M}{\rho k_f}\right)_0.$$

Here the subscript zero refers to the initial conditions and τ_r is a chemical relaxation time of a representative shuffle reaction. This reference time is actually arbitrary in the numerical computations.

With the usual boundary-layer assumptions the momentum equations reduces to

$$\partial p/\partial \eta = 0 \tag{1}$$

	Reaction		A\{cm, mol, s\}	n	E\{cal/mol\}
1	$CH_4 + M \rightleftharpoons CH_3 + H + M$	0·67	$E+18$†	0	88430
2	$CH_4 + O_2 \rightleftharpoons CH_3 + HO_2$	0·8	$E+14$	0	56000
3	$CH_4 + OH \rightleftharpoons CH_3 + H_2O$	0·6	$E+15$	0	12498
4	$CH_4 + H \rightleftharpoons CH_3 + H_2$	0·224	$E+15$	3	8743
5	$CH_4 + O \rightleftharpoons CH_3 + OH$	0·21	$E+14$	0	9061
6	$CH_3 + O_2 \rightleftharpoons H_2CO + OH$	0·12	$E+12$	0	9935
7	$CH_3 + O \rightleftharpoons H_2CO + H$	0·1	$E+15$	0	0
8	$H_2CO + M \rightleftharpoons HCO + H + M$	0·1	$E+15$	0	36759
9	$H_2CO + H \rightleftharpoons HCO + H_2$	0·135	$E+14$	0	3755
10	$H_2CO + O \rightleftharpoons HCO + OH$	0·5	$E+14$	0	4570
11	$H_2CO + OH \rightleftharpoons HCO + H_2O$	0·54	$E+15$	0	6298
12	$HCO + M \rightleftharpoons CO + H + M$	0·5	$E+13$	0	19015
13	$HCO + O \rightleftharpoons CO + OH$	0·1	$E+15$	0	0
14	$HCO + H \rightleftharpoons CO + H_2$	0·2	$E+15$	0	0
15	$HCO + OH \rightleftharpoons CO + H_2O$	0·1	$E+15$	0	0
16	$CO + OH \rightleftharpoons CO_2 + H$	0·4	$E+13$	0	8008
17	$O_2 + H \rightleftharpoons OH + O$	0·6	$E+15$	0	16790
18	$O + H_2 \rightleftharpoons OH + H$	0·32	$E+15$	0	14982
19	$H_2 + O_2 \rightleftharpoons OH + OH$	0·17	$E+14$	0	48150
20	$HO_2 + H \rightleftharpoons OH + OH$	0·25	$E+15$	0	1888
21	$H_2 + OH \rightleftharpoons H_2O + H$	0·29	$E+15$	0	10988
22	$OH + OH \rightleftharpoons H_2O + O$	0·55	$E+14$	0	6994
23	$H + OH + M \rightleftharpoons H_2O + M$	0·84	$E+22$	−2	0
24	$H + O_2 + M \rightleftharpoons HO_2 + M$	0·15	$E+16$	0	−993.6
25	$O + N_2 + M \rightleftharpoons NO + N + M$	0·15	$E+15$	0	75400
26	$N + O_2 \rightleftharpoons NO + O$	0·64	$E+10$	1	6300
27	$N + OH \rightleftharpoons NO + H$	0·4	$E+14$	0	0

† Changed from Bowman's value to fit experimental ignition delay time.

TABLE 1. Reaction mechanism for methane/air oxidation

$$\left\{k_f = AT^n \exp\left(-\frac{E}{RT}\right)\right\}.$$

and the continuity equation for the kth species is

$$-\frac{\eta}{2}\frac{\partial c_k}{\partial \eta} + \frac{\partial j_k}{\partial \eta} = \tau\left(W_k - \frac{\partial c_k}{\partial \tau}\right). \tag{2}$$

Here $c_k = \rho_k/(\rho M_k)$ is the concentration where M_k is the molecular weight and j_k is the mass flux of the kth species. W_k is the mass production rate and is a known function from the reaction equation which describe the reaction mechanism. The reaction scheme (table 1) includes 27 reactions with 17 species.

The energy equation may be written as

$$\frac{\partial}{\partial \eta}\left(c_{p0}\frac{\rho\lambda}{\rho_0\lambda_0}\frac{\partial T}{\partial \eta}\right) + (\eta c_p - 2\sum_k j_k \tilde{c}_{pk})\frac{\partial T}{\partial \eta} = 2\tau\left(c_p\frac{\partial T}{\partial \tau} + \sum_k W_k \tilde{h}_k - \frac{1}{\rho}\frac{\partial p}{\partial \tau}\right). \tag{3}$$

Here $\tilde{c}_{pk} = \partial \tilde{h}_k/\partial T$ and $c_p = \Sigma c_k \tilde{c}_{pk}$; $\tilde{h}_k$ is the molar enthalpy and the other quantities have their usual meaning.

These equations are supplemented by the thermal equation of state

$$p = \rho RT \sum_k c_k. \tag{4}$$

The density field is known from the solution to these equations, after which the velocity u follows from the solution to the global continuity equation

$$-\frac{\eta}{2}\frac{\partial \rho}{\partial \eta} + \rho^2 \frac{\partial \bar{u}}{\partial \eta} = -\tau \frac{\partial \rho}{\partial \tau}; \quad \bar{u} = u\left(\frac{c_{p0} t}{2\lambda_0 \rho_0}\right)^{\frac{1}{2}}. \tag{5}$$

From Hirschfelder, Curtiss & Bird (1967) we find for the mass flux, neglecting Sorret and Dufour effects

$$j_k = \left(\frac{\rho}{\rho_0}\Sigma c_m\right)^2 \sum_n L_n M_n \frac{\partial}{\partial \eta}\left(\frac{c_n}{\Sigma c_m}\right), \quad L_n = \frac{D_{kn} c_{p0} \rho_0}{2\lambda_0}, \tag{6}$$

and for the heat flux

$$\bar{q} = -\frac{c_{p0}}{2}\frac{\rho\lambda}{\rho_0 \lambda_0}\frac{\partial T}{\partial \eta} + \sum_n j_n \tilde{h}_n; \quad \bar{q} = q\left(\frac{c_{p0} t}{2\lambda_0 \rho_0}\right)^{\frac{1}{2}} \tag{7}$$

which was used in (3).

The computation of the heat conduction coefficient λ and the multi-diffusion coefficients D_{kn} are based on potential parameters of the Lennard-Jones potential as mentioned before. For the components Ar, CO_2, O_2, N_2, CO, NO, H_2, H_2O, CH_4 we use the data of Hirschfelder *et al.* (1967) for O and N the data of Morgan & Schiff (1964) and for H the data of Khouw, Morgan & Schiff (1969). Potential parameter for the components HCO, H_2CO, CH_3, OH and HO_2 could not be found in the literature and the parameters for the similar molecules CO, CH_4, H_2O and O_2 were used respectively.

In equilibrium flow and frozen flow ($\tau_r \to 0$ or $\tau_r \to \infty$ respectively) the dependence on τ vanishes. These flows are self-similar. In equilibrium flow, the expressions τW_k remain finite and may be computed from the left-hand side of equation (2) using the equilibrium concentrations $c_{ke}(\rho, T)$.

3. Boundary and initial conditions

The similarity solutions for frozen flow and equilibrium flow require time-independent boundary conditions. As was mentioned in the introduction, the boundary conditions far away from the wall are time-dependent even in non-reacting flow and this introduces a time scale into the problem which precludes in general a similarity solution. However, if this characteristic time is large compared with the diffusion time, the boundary conditions are quasi-steady and we expect a quasi-similar solution of the form $\rho(x,t)/\rho_\infty(t) = f(\eta)$, if t is replaced by

$$t' = \int_0^t \alpha_\infty(t)/\alpha_0 \, dt, \quad \alpha = \lambda/\rho c_p$$

in the similarity variable η (Vrugt 1976).

It is appropriate at this stage to look at the density behaviour outside the boundary layer. In figure 1 the density history at a position 14 mm from the wall is given for a pure argon flow. In a pure argon flow we would expect the direct interaction of the shock with the boundary layer to be small (Strehlow & Cohen 1959) and the pressure traces (not shown here) give no indication of the shock bifurcation, typical for this interaction. In figure 1 the density increases with time and its history may be fitted

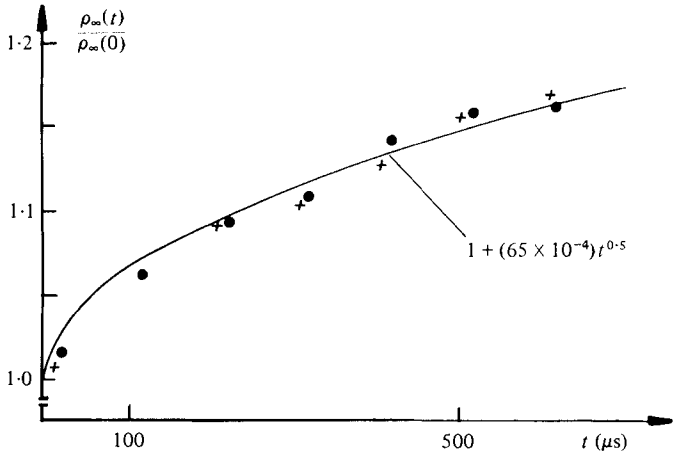

FIGURE 1. Density variation in the outer flow at 14 mm from the end wall from an experiment using argon. The two symbols, ●, +, indicate different tests.

to an equation $\rho_\infty(t)/\rho(0) = 1 + Kt^{0.5}$ suggesting that the change in density is due to perturbation in the flow properties ahead of the reflected shock, caused by laminar boundary layer behind the incident shock (Dyner 1966). If we exclude the immediate neighbourhood of the time origin the characteristic time $(\rho(\partial\rho/\partial t)^{-1})$ say, is in the order of milliseconds and this time is large compared to the diffusion time, which in laminar flow, is equal to actual time. In figure 2 the density distribution in the boundary layer is given as a function of the similarity variable $\tilde{\eta} = x/(2\alpha t')^{\frac{1}{2}}$; the use of this spatial similarity variable instead of the material similarity variable η avoids the necessity of integrating the experimental density distribution. Figure 2 shows that similarity is indeed obtained and also, that good agreement exists between theory and experiment. The coefficient of thermal conductivity λ used in figure 2 is a fit to λ computed on the basis of Lennard-Jones potential and gives $\lambda \sim T^{\nu}$ with $\nu = 0{\cdot}668$. It is worth mentioning that this exponent gave a better agreement with the experimental data than the exponent $\nu = 0{\cdot}75$ recommended by Amdur & Mason (1958). The free-stream temperature used in reducing the data in figure 2 was determined from the measured free-stream density and the measured pressure.

In order to discuss the boundary conditions for the tests with combustible mixture we note from figure 3 that the density outside the boundary layer has a similar behaviour as the pure argon case during ignition delay time (results of several tests differ slightly in ignition delay time, caused by small differences in shock velocity).

While we expect for this mixture a direct shock boundary layer interaction even though the mixture is diluted, no decrease in density is observed. The pressure trace measured 5 mm from the end wall shows no indication of bifurcation of the reflected shock, but a trace measured at 46 mm does. We conclude from this, that the condition near the wall are mostly determined by the inhomogeneities ahead of the reflected shock and by the vibrational relaxation of the oxygen component. The expected density rise due to this particular relaxation is indicated on figure 3. The chemical relaxations proceeding during ignition delay time namely the start reactions (reaction 1 and 2 of table 1) have only a small effect on the flow. The density again may be fitted to an equation of the form $\rho_\infty(t)/\rho(0) = 1 + Kt^N$, where the exponent N is now not

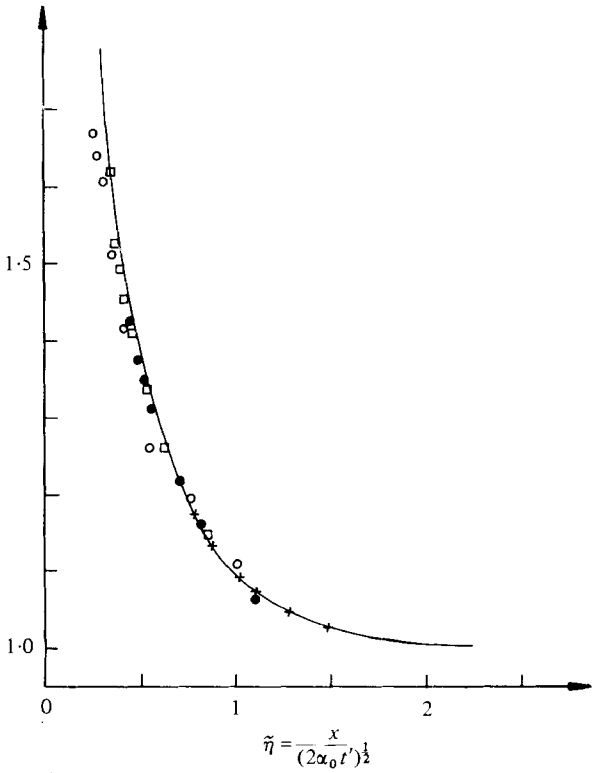

FIGURE 2. Similarity solution for the argon boundary layer. Theory, ρ/ρ_0: ——. Experiment, $\rho/\rho_\infty(t)$: +, x = 1·3 mm; ●, x = 0·7 mm; □, x = 0·53 mm; ○, x = 0·36 mm.

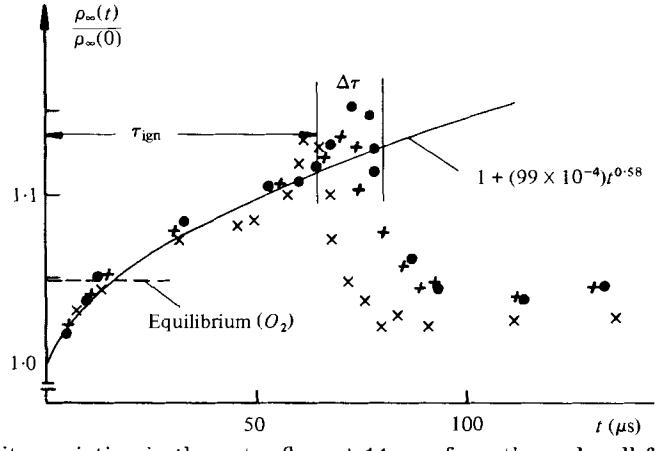

FIGURE 3. Density variation in the outer flow at 14 mm from the end wall from an experiment using the mixture of gases. τ_{ign} is the ignition delay time; $\Delta\tau$ is the variation of τ_{ign}. The symbols, ●, ×, +, indicate different tests.

exactly 0·5. If we ignore, as before early times, the typical time of the density change during ignition delay time is in the order of milliseconds and the boundary layer during this time behaves quasi-similarly. After ignition delay time, there is a rather rapid change of density due to the combustion process and the boundary layer development is no longer quasi-similar. Time dependent boundary condition must be

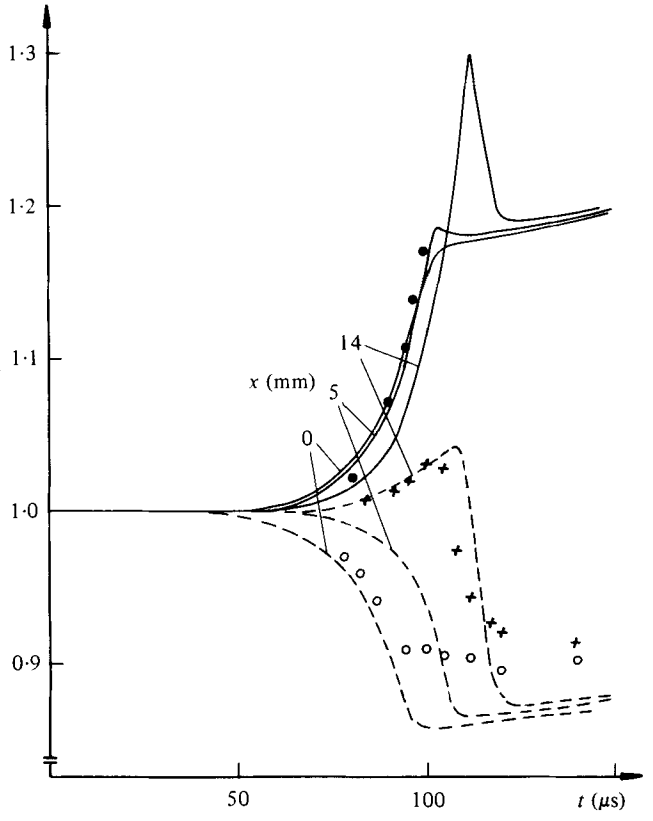

FIGURE 4. Comparison between theoretical and experimental density and pressure histories in the outer flow. At $t = 0$, $T_0 = 2017$ K, $p_0 = 0{\cdot}519$ bar, $X[CH_4] = 0{\cdot}325$, $X[O_2] = 0{\cdot}162$, $X[N_2] = 0{\cdot}0993$, $X[Ar] = 0{\cdot}7062$. Theory: ——, p/p_0; – – – –, ρ/ρ_0. Experiment: ●, p/p_0, $x = 5$ mm; +, $\rho/\rho_\infty(t)$, $x = 14$ mm; ○, $\rho/\rho_\infty(t)$, $x = 1$ mm.

prescribed. While it is of course possible to include in these also the time dependence of the boundary conditions during ignition delay time, it is better to exploit the self-similar nature of the flow during this time in order to exhibit clearly the changes in the boundary layer resulting from the combustion process. We shall therefore account for the viscous interaction process during ignition delay time by referring the data to the slowing varying data outside the boundary layer.

The boundary conditions may then be determined on the basis of inviscid one-dimensional reacting flow and solved for as an initial and boundary-value problem by the method of characteristics. From the measured incident shock velocity, the condition behind the reflected shock are computed under the assumption that the gas is in vibrational equilibrium, frozen chemistry, and at rest. The assumption of vibrational equilibrium in the oxygen component is consistent with the fact that equilibrium of this mode occurs during the quasi-similar period.

Figure 4 shows a comparison of density histories at $x = 14$ mm and $x = 1$ mm (before the boundary layer has reached this station) and pressure history at 5 mm with the results of the characteristics computation. The agreement is quite good and supports our contention that viscous interaction and vibrational non-equilibrium in the oxygen component can be corrected for, and plays a role only before onset of the

fast energy producing reactions. The results of this computation at $x = 0$ should properly be used as boundary conditions for the boundary-layer solution. But since there is a difference of about 5 % in the final density, doing so, would impose a boundary condition already in error by 5 %. We therefore determine the boundary conditions from the system of equations which results from the boundary-layer equation, when the gradients of concentration, temperature and density are set equal to zero. One variable must then be specified and we choose the experimental density outside the boundary layer at $x = 1{\cdot}0$ mm, that is before the edge of the boundary layer has reached this position.

The initial conditions are the conditions behind the reflected shock. The boundary conditions near the wall for the boundary-layer computation require the velocity to vanish there and then any temperature jump, as mentioned, can be neglected. The wall temperature moreover remains practically constant, since the Fourier number of the conduction process in the wall is very small (Clarke 1962).

For non-equilibrium boundary layer we assume a non-catalytic wall, i.e. we set the concentration gradients at the wall equal to zero, the concentrations then change at the wall due to the diffusion process and the flow will become an equilibrium flow.

In equilibrium flow the concentrations in the boundary layer are functions of temperature and in general boundary conditions for concentrations or their derivatives cannot be satisfied. (Specifying boundary conditions in this case gives rise to non-equilibrium layer in the immediate neighbourhood of the wall (Hirschfelder 1957). In the case discussed here the equilibrium flow satisfies the conditions of vanishing gradients at the wall. Even if this were not the case the effect of Hirschfelder layer would be very small.

For frozen flow, the wall concentrations for all times are set equal to the initial concentrations. The initial concentrations themselves are independent of η and are given for both, frozen and equilibrium flow by the corresponding concentrations outside of the boundary layer.

With constant initial concentrations equal to wall concentrations the concentrations in the boundary layer will not change in frozen flow and the gradients of concentrations remain zero at the wall. This behaviour is also expected for non-equilibrium flow near $\tau = 0$. In fact, the self-similar solution to the frozen flow provides the initial conditions for the non-equilibrium flow as can be seen from equations (2) and (3).

4. Numerical solutions

The self-similar flows are two-point boundary-value problems and solved by the finite-difference method of Blottner (1970). The numerical results have been checked by recomputing the flow as initial-value problems with the so called 'shooting' technique using the heat flux and the diffusion fluxes at $\eta = 0$ from the finite-difference solution.

The non-equilibrium flow is computed by firstly approximating the time derivatives by backward differences and treating the resulting system of ordinary differential equations by Blottner's (1970) method.

The heat flux can be found from (7) by numerical differentiation of the solution

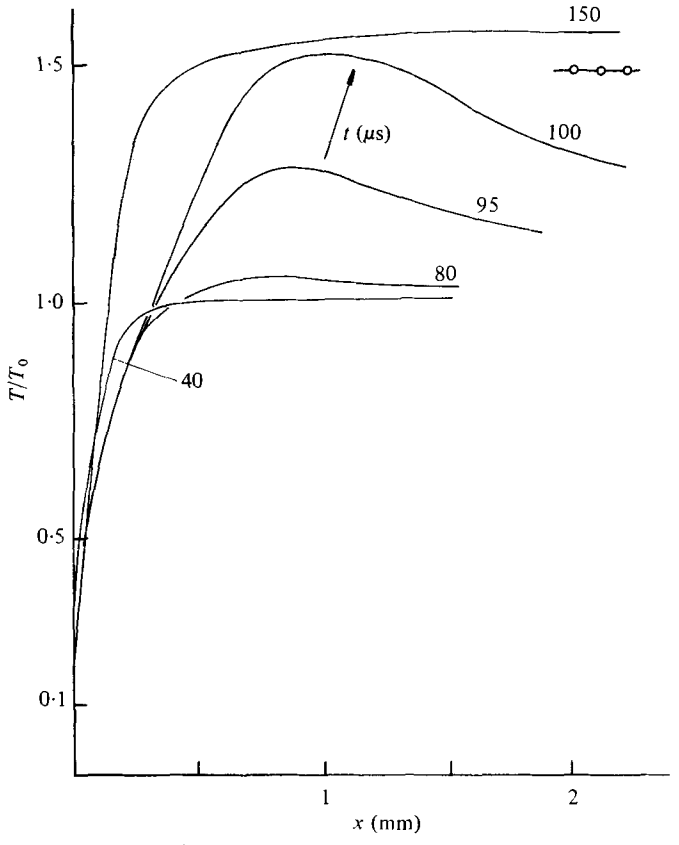

FIGURE 5. Temperature in the non-equilibrium boundary-layer. At $x = 0$, $T_w = 300$ K, $\partial c_k/\partial x = 0$. As $x \to \infty$, there is isobaric combustion. At $t = 0$, $T_0 = 2000$ K, $p_0 = 1$ bar, $X[\mathrm{Ar}] = 0{\cdot}7$, $X[\mathrm{CH_4}] = 0{\cdot}07$, $X[\mathrm{O_2}] = 0{\cdot}14$, $X[\mathrm{N_2}] = 0{\cdot}09$.

profiles once the finite difference solution is known. Alternatively it may be computed from the integral form of the energy equation. The appropriate form is given by

$$q(0,t) = q(\eta_e,t) + \left(\frac{2\lambda_0\rho_0}{c_{p0}t}\right)^{\frac{1}{2}}\left\{\int_0^{\eta_e}\left(-\frac{\eta}{2}\frac{\partial h}{\partial \eta} + t\frac{\partial h}{\partial t}\right)d\eta - t\frac{\partial p}{\partial t}\int_0^{\eta_e}\frac{d\eta}{\rho}\right\}. \tag{8}$$

The difference between the fluxes computed from both methods is used as an additional check for the numerical computation.

Figure 5 shows an interesting aspect of the results from numerical computation. The temperature as a function of the physical distance x shows a frozen boundary layer up to $t = 40\,\mu$s, and a near-equilibrium boundary layer at $t = 150\,\mu$s. For intermediate times the temperature is no longer monotonic but shows transient maxima, indicating that the combustion proceeds faster in the boundary layer. Spurk (1980) has shown that this effect can be expected whenever chemical reactions and diffusion occur simultaneously.

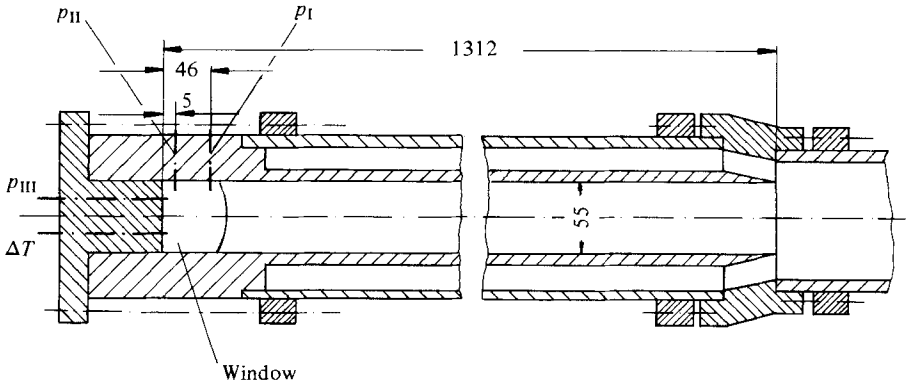

FIGURE 6. Test section with positions of pressure gauges p_I–p_{III}, and temperature gauges.

5. Experiments

Figure 6 shows the test section of a shock tube used in these experiments. The test section consists of an insert having a square cross-section, 55 × 55 mm, which is fitted into a conventional round cross-section pressure driven shock tube. This insert reduces boundary-layer effects behind the incoming shock and allows interferometric observation of the flow through windows mounted in the side walls. The test gas, whose composition has been determined by mass spectroscopy to $X[CH_4] = 0{\cdot}0325$, $X[O_2] = 0{\cdot}162$, $X[N_2] = 0{\cdot}0993$ and $X[Ar] = 0{\cdot}7062$ is filled in the tube to an initial pressure of 7 mbar.

Shock waves with Mach-numbers of about 3·2 heat the test gas up to 2200 K upon reflection from the end wall.

The change in index of refraction in the developing boundary layer at the end wall is measured by a focused laser beam. The laser beam is passed through a Mach Zehnder interferometer where the beam is split into a reference beam and the beam traversing the boundary layer in the test section. At the exit of the interferometer, the two beams are again superimposed and interfere. In an adjustment, where all interferometer plates and mirrors are parallel, the intensity of the beam will vary in time between complete extinction and maximum intensity depending on the phase difference $\phi(t)$ between the two beams. The phase difference is found from the recorded intensity.

$$I = I_0 \cos^2 \tfrac{1}{2}\phi(t)$$

as viewed by a photodiode. The beam is adjusted parallel to the end wall at distances between 0·3 and 1·5 mm. Optical stops in the light pass allow a spatial resolution of about 0·1 mm and reduce effects of diffraction caused by gradients of the refractive index in the boundary layer. An additional beam outside the boundary layer is placed at a distance of 14 mm from the end wall.

For the phase difference at reference time $t = 0$ and at time t we have

$$\phi(t) - \phi(0) = \frac{2\pi}{\bar{\lambda}} \int_0^L (n(s,t) - n(s,0))\, ds$$

where $\bar{\lambda}$ is the observing wavelength, s is the integration path and L its length occupied by the test gas. If the gradients are normal to the beam, the refractive index n is independent of s, and may be determined from

$$n(t) - n(0) = (\phi(t) - \phi(0))\, \bar{\lambda}(2\pi L)^{-1}. \tag{9}$$

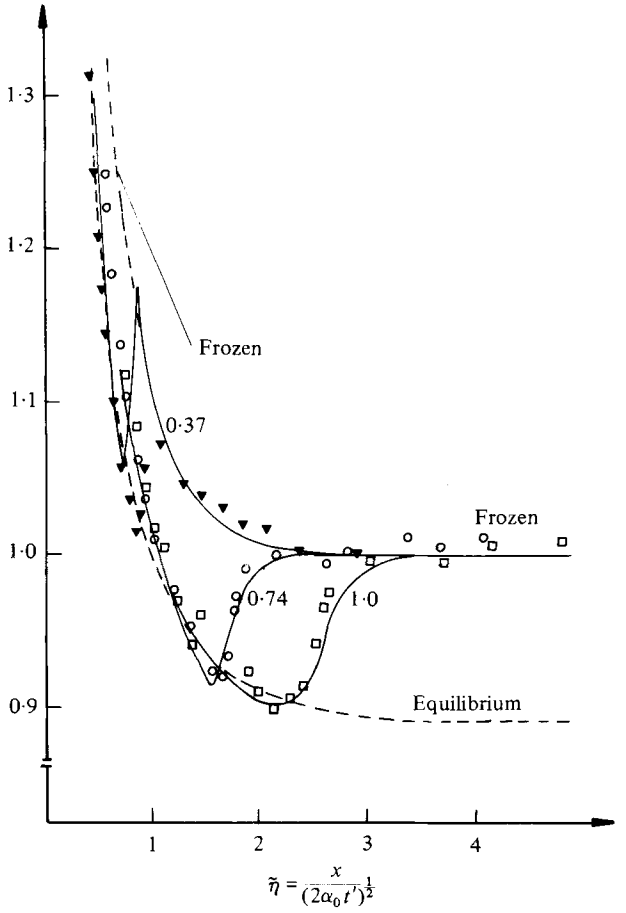

FIGURE 7. Comparison between theoretical and experimental density traces in the non-equilibrium boundary layer. At $x = 0$, $T_w = 300$ K, $\partial c_k/\partial x = 0$. As $x \to \infty$, there is homogeneous combustion with density known from experiment. At $t = 0$, $T_0 = 2017$ K, $p_0 = 0{\cdot}519$ bar, $X[CH_4] = 0{\cdot}0325$, $X[O_2] = 0{\cdot}162$, $X[N_2] = 0{\cdot}099$, $X[Ar] = 0{\cdot}7062$. Theory: ——, ρ/ρ_0. Experiment, $\rho/\rho_\infty(t)$: □, $x = 1{\cdot}0$ mm; ○, $x = 0{\cdot}74$ mm; ▼, $x = 0{\cdot}37$.

The measured index of refraction may then be compared with predictions from the equation

$$n(t) = 1 + \sum_i K_i \rho_i(t). \tag{10}$$

Since the index of refraction for this mixture of gases is almost independent of gas composition as the actual computations show and depends only on the overall density, a fact also noted in high temperature air (Spurk 1970), we give the results of the experiments in terms of density

$$\rho(t) = (n(t) - 1)/K_g; \quad K_g = \sum_i K_i \rho_i/\rho \simeq \text{const.}$$

The Gladstone–Dale constants K_i for the different species were taken from Borchers *et al.* (1962), Alpher & White (1959) and White (1961), except for the components CH_3, H_2CO, HCO and H_2O for which the same value as those for CH_4, CO and O_2

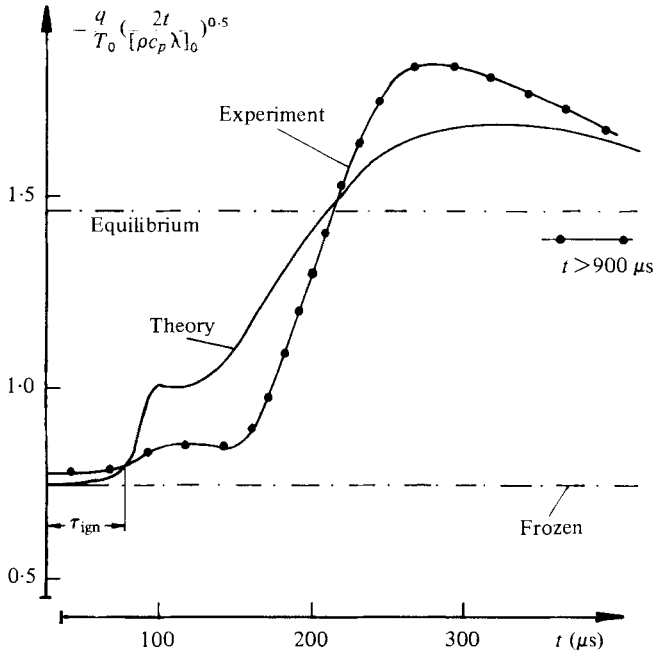

FIGURE 8. Comparison of computed and measured heat flux to the wall. At $x = 0$, $T_w = 300$ K, $\partial c_k/\partial x = 0$. As $x \to \infty$, there is homogeneous combustion with density known from experiment. At $t = 0$, $T_0 = 2017$ K, $p_0 = 0{\cdot}519$ bar, $X[CH_4] = 0{\cdot}0325$, $X[O_2] = 0{\cdot}162$, $X[N_2] = 0{\cdot}0993$, $X[Ar] = 0{\cdot}7062$.

respectively were used. A more complete description of the experimental set-up is given by Keiper (1980).

6. Comparison of experiments with theory

Figure 7 shows a comparison of the density distribution in the boundary layer in the similarity variable $\tilde{\eta} = x/(2\alpha_0 t')^{\frac{1}{2}}$. The two traces at $x = 1{\cdot}0$ mm and $x = 0{\cdot}74$ mm are two different tests with the same ignition delay time.

The agreement between theory and experiment is excellent. The results show that boundary layer behaves as a frozen boundary layer until the flame front reaches the measuring position. The flame front then causes a rapid change of index of refraction (or density). The experimental points then indicate an equilibrium boundary layer. We also show experimental points for a trace at $x = 0{\cdot}37$ mm, but this test had a different ignition delay time and therefore a different density history outside the boundary layer than the history on which the computation are based. While we cannot make a quantitative comparison here, the experimental points follow the frozen curve until the flame front reaches the measuring position. For large times, the experimental data then follow the equilibrium curve.

Figure 8 shows the comparison between theory and experiment for the heat flux into the end wall. During ignition delay time there is good quantitative agreement between measurement and theory. For long times ($t > 400\ \mu s$) theory and experiment again appear to converge. In the interesting time between 150 and 300 μs there are substantial differences between theory and experiment. Of these the most significant

	Reaction		A[cm, mol, s]	n	E[cal/mol]
1	$CH_3 + CH_3 \rightleftarrows C_2H_6$	0·4	$E+53$	−12	16200†
2	$CH_3 + CH_3 \rightleftarrows C_2H_5 + H$	0·8	$E+15$	0	26512
3	$CH_3 + CH_3 \rightarrow C_2H_4 + H_2$	0·1	$E+17$	0	32005
4	$C_2H_6 + H \rightleftarrows C_2H_5 + H_2$	0·54	$E+3$	3·5	5207
5	$C_2H_6 + O \rightleftarrows C_2H_5 + OH$	0·3	$E+8$	2	5111
6	$C_2H_6 + OH \rightleftarrows C_2H_5 + H_2O$	0·63	$E+7$	2	645
7	$C_2H_5 \rightleftarrows C_2H_4 + H$	0·14	$E+39$	−7	59500†
8	$C_2H_4 + O \rightleftarrows CH_3 + HCO$	0·2	$E+14$	0	2293
9	$C_2H_4 + OH \rightleftarrows CH_3 + H_2CO$	0·7	$E+36$	−7	9100†

† Value for 1 bar.

TABLE 2. Reaction scheme for higher hydrocarbons.

one is the steeper increase of heat flux during this time. The numerical computation show here maxima in the radical concentrations near the wall. If the radicals cannot exist near the wall but react very fast near the wall there would be additional contribution to the heat flux due to the diffusion of radicals to the wall. Some sample computations were made assuming that the surface is catalytic to hydrogen atom recombination; these showed a slight decrease of the conductive flux and positive contribution to the heat flux resulting from diffusion. Both effects nearly cancelled and no change occurred in the overall flux.

It is worth pointing out that Bowman's reaction mechanism is a high temperature mechanism which may not be valid near the cold wall. In this region, recombination reactions may occur which lead to higher hydrocarbons (Warnatz 1980). Computation based on Bowman's scheme together with nine reactions (table 2) from Warnatz did not give significant change in heat flux as compared to computation without these reactions.

7. Conclusions

The very close agreement between the theoretical and experimental density profiles in the boundary layer strongly suggests that this boundary layer, undergoing an exothermic reaction, is laminar and that the theory describes adequately the coupled process of chemical relaxation and transport processes. Experiment and theory show the existence of quasi-similar solutions for short and long times, despite substantial changes in conditions outside the boundary layer. While agreement between theoretical and experimental heat transfer data is satisfactory there are typical differences which cannot be explained at the present time. It is likely that the difference in heat transfer is due to catalytic action of the wall, this could indeed make contributions to the heat transfer in the right direction. The agreement in density profiles of course is not sufficient to judge details of reaction mechanism since the density is not sensitive to the gas composition, and it would be most desirable to have in addition concentration profiles of one or more species.

REFERENCES

ALPHER, R. A. & WHITE, D. R. 1959 Optical refractivity of high-temperature gases I. *Phys. Fluids* **2**, 153.

AMDUR, I. & MASON, E. A. 1958 Properties of gases at very high temperatures. *Phys. Fluids* **1**, 361.

BAGANOFF, D. 1965 Experiments on the wall-pressure history in shock-reflexion processes. *J. Fluid Mech.* **23**, 209.

BLOTTNER, F. G. 1970 Finite difference methods of solution of the boundary-layer equations. *A.I.A.A. J.* **8**, 193.

BORCHERS, H., HAUSEN, H., HELLWEGE, K.-H. & SCHÄFER, KL. 1962 *Numerical Data and Functional Relationships in Physics, Chemistry, Astronomy, Geophysics, and Technology, Volume* II. *Part* 8. *Optical Constants*, pp. 6–871. Springer: Landolt-Börnstein. (In German.)

BOWMAN, G. T. 1974 Non-equilibrium radical concentrations in shock-initiated methane oxidation. *15th Symp. (Int.) on Combustion*, p. 869. The Combustion Institute.

CLARKE, J. F. 1962 Temperature-time histories at the interface between gas and a solid. *J. Fluid Mech.* **13**, 47.

DYNER, H. B. 1966 Density variation due to reflected shock–boundary-layer interaction. *Phys. Fluids* **9**, 879.

FAY, J. A. & KEMP, N. H. 1965 Theory of heat transfer to a shock-tube end-wall from an ionized monatomic gas. *J. Fluid Mech.* **21**, 659.

HIRSCHFELDER, J. O. 1957 Heat transfer in chemically reacting mixtures. *J. Chem. Phys.* **26**, 274.

HIRSCHFELDER, J. O., CURTISS, C. F. & BIRD, R. B. 1967 *Molecular Theory of Gases and Liquids*, pp. 516, 1110. Wiley.

KEIPER, R. 1980 Theoretische und experimentelle Untersuchung der Temperaturgrenzschicht mit chemischen Reaktionen unter dem Einfluß der Transportprozesse. Diss. Darmstadt D 17, p. 109.

KHOUW, B., MORGAN, J. E. & SCHIFF, H. I. 1969 Experimental measurements of the diffusion coefficients of H atoms in H_2 and H_2–He and H_2–Ar mixtures. *J. Chem. Phys.* **50**, 66.

MARK, M. 1953 The interaction of a reflected shock wave with the boundary layer in a shock tube. *N.A.C.A. Tech. Memo.* 1418.

MORGAN, J. E. & SCHIFF, H. I. 1964 Diffusion coefficients of O and N atoms in inert gases. *Canad. J. Chem.* **42**, 2300.

NELSON, H. F. 1976 Nitric oxide formation in combustion. *A.I.A.A. J.* **14**, 1177.

RUDINGER, G. 1961 Effect of boundary-layer growth in a shock tube on shock reflection from a closed end. *Phys. Fluids* **4**, 1463.

PRESLEY, L. L. & HANSON, R. K. 1969 Numerical solutions of reflected shock-wave flow fields with non-equilibrium chemical reactions. *A.I.A.A. J.* **7**, 2267.

SPURK, J. H. 1970 Experimental and numerical non-equilibrium flow studies. *A.I.A.A. J.* **8**, 1039.

SPURK, J. H. 1980 Bemerkungen zur thermischen Nichtgleichgewichtsgrenzschicht. *Ing. Archiv* **49**, 269.

STREHLOW, R. A. & COHEN, A. 1959 Limitations of the reflected shock technique for studying fast chemical reactions and its application to the observation of relaxation in nitrogen and oxygen. *J. Chem. Phys.* **30**, 257.

STURTEVANT, B. & SLACHMUYLDERS, E. 1964 End-wall heat-transfer effects on the trajectory of a reflected shock wave. *Phys. Fluids* **7**, 1201.

VRUGT, P. J. 1976 Shock tube study of the coefficient of thermal conductivity of helium, neon, argon and krypton. Ph.D. thesis, Eindhoven University of Technology, p. 100.

WARNATZ, J. 1980 The structure of laminar alkane-, alkene-, and acetylene flames. *18th Symp. (Int.) on Combustion, Waterloo, Canada.*

WHITE, D. R. 1961 Optical refractivity of high temperature gases III. *Phys. Fluids* **4**, 40.